Supplementary Information for

Parallel Labeled-Line Organization of Sympathetic Outflow for Selective Organ Regulation in Mice

Yukiko Harima*, Masafumi Tsurutani, Serika Yamada, Shuntaro Uchida, Kengo Inada, Mitsue Hagihara, Satsuki Irie, Mayo Shigeta, Takaya Abe, Yukiko U. Inoue, Takayoshi Inoue, and Kazunari Miyamichi*

*Correspondence: Yukiko Harima; Kazunari Miyamichi

E-mail: yukiko.harima@riken.jp (H.Y.); kazunari.miyamichi@riken.jp (K.M.)

This PDF file includes:

Supplementary Figures 1 to 7

Supplementary Table 1

Supplementary References

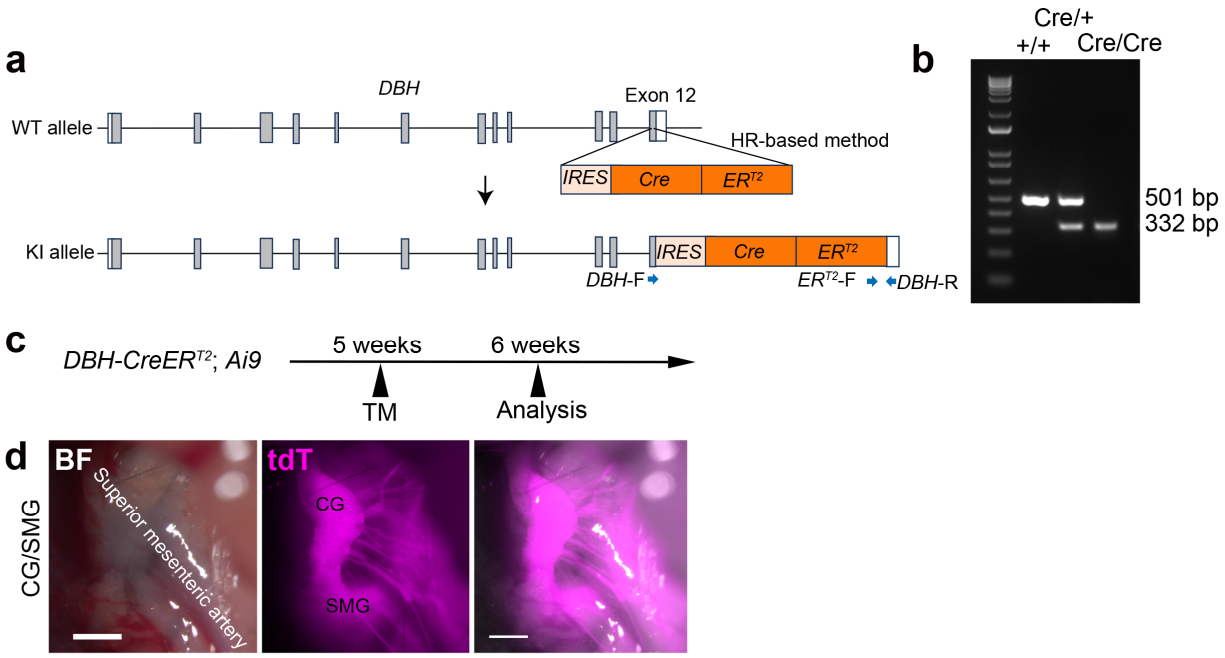

Supplementary Fig. 1: Labeling post-GNs in the CG/SMG via *DBH-CreER^{T2}* mice, related to Fig. 1.

a, Illustration of the knock-in (KI) strategy for generating *dopamine-β-hydroxylase* (*DBH*)-*CreER*^{T2} mice using the homologous recombination (HR)-based method[1]. The *DBH* gene comprises 12 exons, with open and closed boxes denoting untranslated and protein-coding regions, respectively. The KI allele is schematically depicted below, where the *IRES-Cre-ER^{T2}* cassette is inserted into the coding end of the *DBH* locus located in exon 12. Blue arrows indicate the site of genotyping primer sites. **b**, Representative gel image of electrophoresis examining the *Cre* allele and a negative control (wild-type animal). **c**, Time line of the experiments for genetically labeling postganglionic neurons. TM, tamoxifen. **d**, Fluorescence microscope imaging of the CG/SMG in *DBH-CreER^{T2}; Ai9* mice. BF, bright field. tdT, tdTomato from the *Ai9* allele. Scale bar, 1 mm.

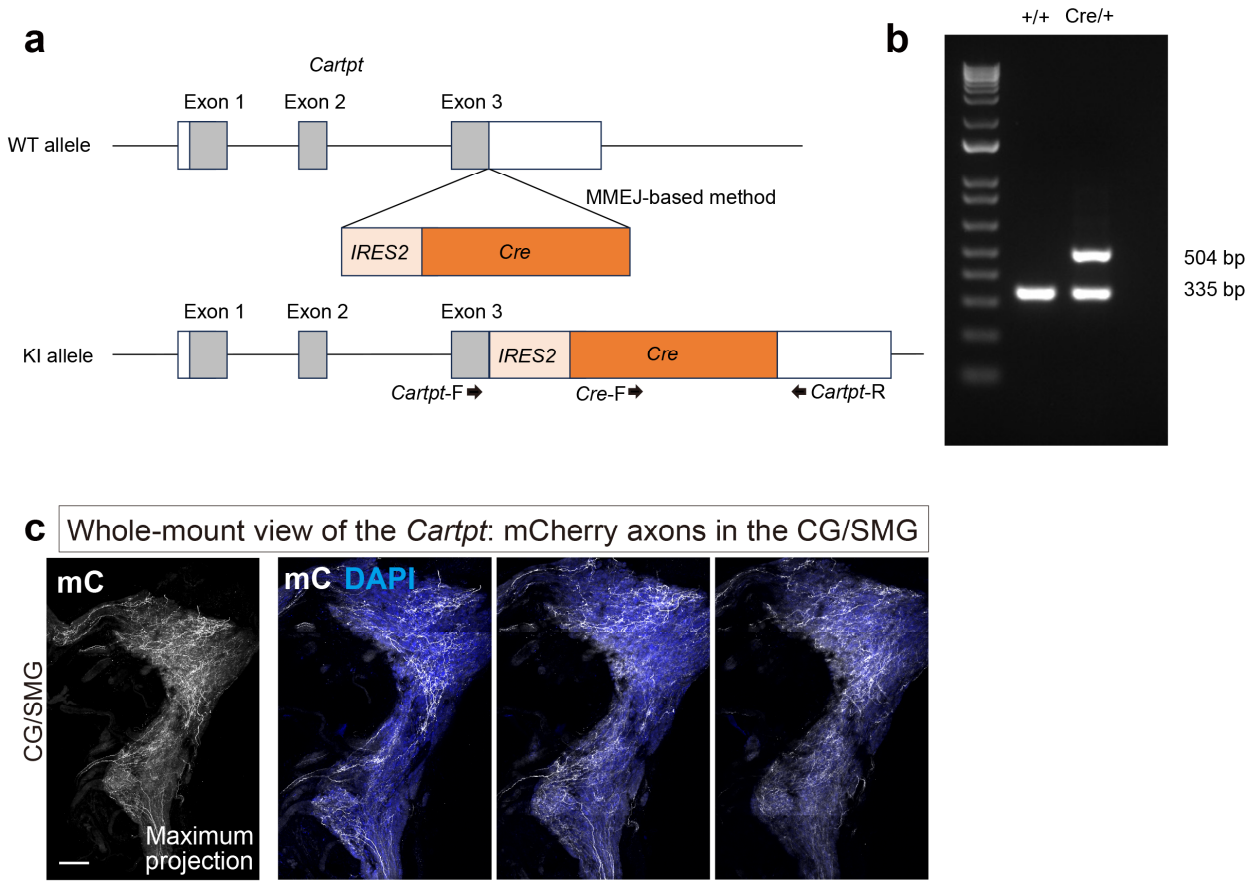

Supplementary Fig. 2: Generation of *Cartpt-Cre* mice, related to Fig. 2.

a, Illustration of the knock-in (KI) strategy for generating *Cartpt-Cre* mice using the microhomology-mediated end joining (MMEJ)-based method[1]. Top: The *Cartpt* gene comprises three exons, where open and closed boxes denote untranslated and protein-coding regions, respectively. The *IRES2-Cre* cassette was inserted immediately downstream of the coding end of *Cartpt* on exon 3. Bottom: Schematic representation of the KI allele. Black arrows indicate the location of genotype primers. **b**, Representative gel image displaying electrophoresis results examining the *Cre* allele and negative control (wild-type animal). **c**, Representative whole mount view showing the mCherry+ axonal distribution of *Cartpt*+ SPNs located in the T8–12 SC segments (corresponding to data in Fig. 2c, d). The left panel presents the maximum projection image of Z-stacks for the mCherry channel, while the right three panels display distinct Z-positions. Scale bar, 200 µm. These data suggest the widespread axonal distribution of *Cartpt*+ SPNs across the entire CG/SMG.

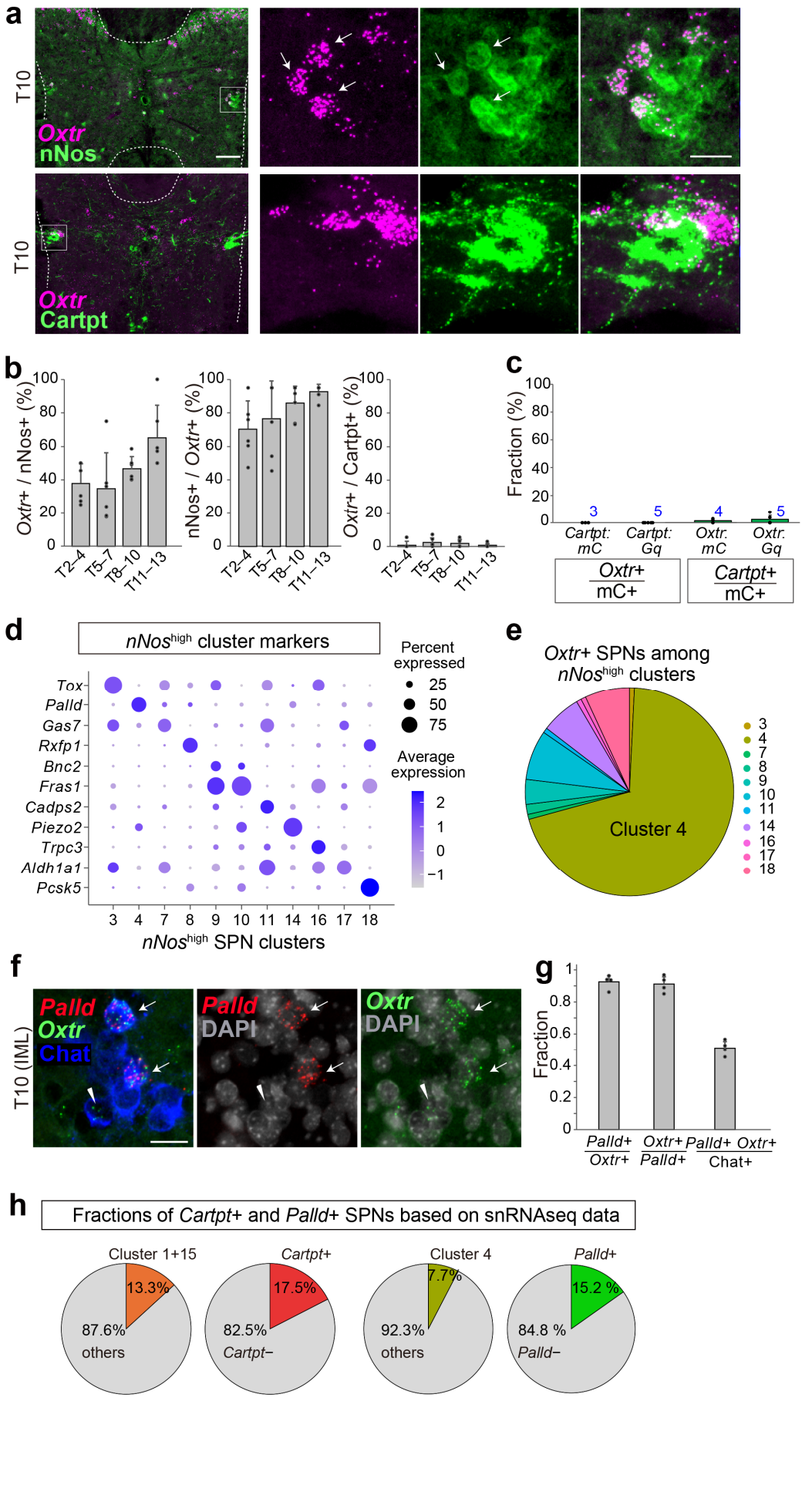
a
T10
Oxtr
nNos
T10
Oxtr
Cartpt
b
Oxtr+ / nNos+ (%)
nNos+ / Oxtr+ (%)
Oxtr+ / Cartpt+ (%)
T2–4
T5–7
T8–10
T11–13
c
Fraction (%)
3
5
4
5
Cartpt: mC
Cartpt: Gq
Oxtr: mC
Oxtr: Gq
Oxtr+ / mC+
Cartpt+ / mC+
d
nNos^high cluster markers
Percent expressed
25
50
75
Average expression
2
1
0
−1
Tox
Palld
Gas7
Rxfp1
Bnc2
Fras1
Cadps2
Piezo2
Trpc3
Aldh1a1
Pcsk5
3 4 7 8 9 10 11 14 16 17 18
nNos^high SPN clusters
e
Oxtr+ SPNs among nNos^high clusters
Cluster 4
3
4
7
8
9
10
11
14
16
17
18
f
T10 (IML)
Palld
Oxtr
Chat
Palld
DAPI
Oxtr
DAPI
g
Fraction
Palld+ / Oxtr+
Oxtr+ / Palld+
Palld+ / Chat+
Oxtr+
h
Fractions of Cartpt+ and Palld+ SPNs based on snRNAseq data
Cluster 1+15
13.3%
87.6%
others
Cartpt+
17.5%
82.5%
Cartpt−
Cluster 4
7.7%
92.3%
others
Palld+
15.2 %
84.8 %
Palld−

Supplementary Fig. 3: *Oxtr* marks a *nNos*+ TC type corresponding to cluster 4, related to Figs. 2 and 3.

a, Expression of *Oxtr* mRNA (magenta) and nNos or Cartpt immunostainings (green) in the T10 SC of wild-type mice, with magnified and channel-separated images corresponding to the white-boxed area. Arrows indicate *Oxtr* and nNos dual-positive cells. Scale bars, 100 μm for the left images and 25 μm for the magnified images. **b**, Percentage of *Oxtr*+ cells among nNos+ cells (left), nNos+ cells among *Oxtr*+ cells (middle) in the IML regions, and *Oxtr*+ cells among Cartpt+ cells (right) in the IC, CA, and IML regions. N = 6 mice. **c**, Percentage of mC+ cells in *Cartpt-Cre* mice that express *Oxtr* mRNA (left) and in *Oxtr-Cre* mice that express *Cartpt* mRNA (right). The expression of mC was induced using AAV8-*hSyn-DIO-mCherry* (as in Fig. 2**c**) and AAV8-*hSyn-DIO-Gq-mCherry* (as in Fig. 3**c**). The number of animals (N) is indicated in blue within the panel. **d**, Identification of enriched differentially expressed genes among $nNos^{high}$ clusters, as in Fig. 1**i**. **e**, Pie chart displaying the fraction of *Oxtr*+ SPNs detected within each $nNos^{high}$ SPN cluster. The majority of *Oxtr*+ SPNs are found in cluster 4. **f**, Expression of *Palld* (red, a cluster 4 marker) and *Oxtr* (green) mRNAs detected by RNAscope, along with Chat immunostaining (blue) and DAPI staining in the IML of the T10 spinal segment of wild-type mice. Arrows indicate *Palld*, *Oxtr*, and Chat triple-positive cells, while the arrowhead depicts a *Palld*– *Oxtr*+ Chat+ cell. Scale bars, 25 μm. **g**, Percentage of *Palld*+ cells among *Oxtr*+ cells (left), *Oxtr*+ cells among *Palld*+ cells (middle), and *Palld*+ *Oxtr*+ dual-positive cells among Chat+ cells (right) in the IML of the T8–T13 segments. N = 4 mice. **h**, Fraction of SPN clusters 1+15 among all SPN clusters, *Cartpt*+ SPNs among all SPNs, SPN cluster 4 among all SPN clusters, and *Palld*+ SPNs among all SPNs, based on published transcriptome data[2]. These data suggest that the majority of *Cartpt*+ SPNs are included in the $nNos^{low}$ SPN clusters 1 and 15, while *Palld*+ (*Oxtr*+) SPNs may have a slightly broader distribution beyond $nNos^{high}$ SPN cluster 4. Error bars, SD. Source data are provided as a Source Data file.

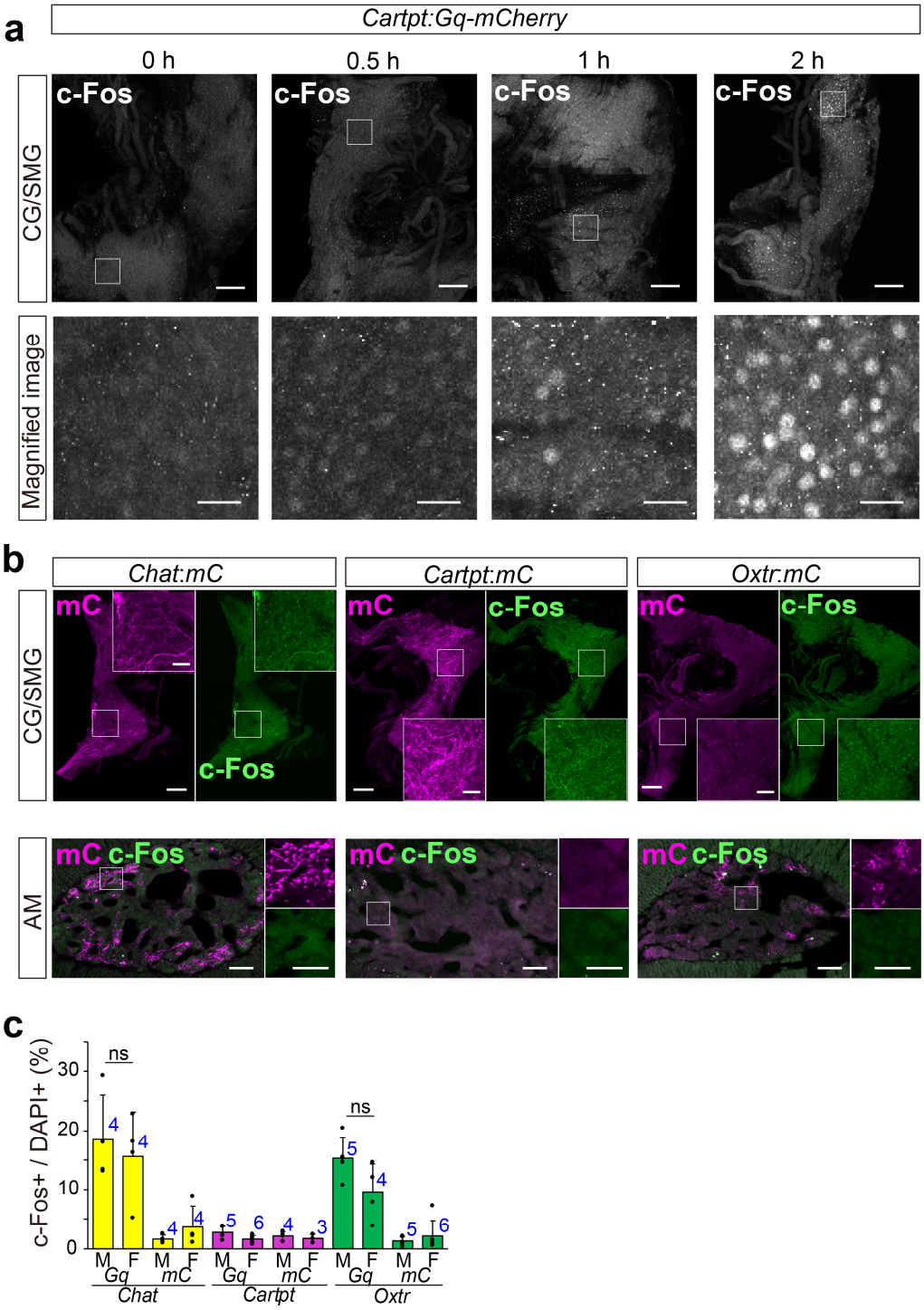

Supplementary Fig. 4: Time course and control experiments for the activation of specific SPNs, related to Fig. 3.

a, Expression of c-Fos (gray) in the whole mount view of the CG/SMG is shown at various time points (0, 0.5, 1, or 2 hours) following CNO administration in *Cartpt-Cre* mice injected with AAV8-*hSyn-DIO-Gq-mCherry* into the T8–T12 SC. Lower panels display magnified images within the white-boxed areas. Scale bars, 200 µm for the top images and 50 µm for the magnified images. **b**, Expression of c-Fos (green) in the whole mount view of the CG/SMG (upper) and adrenal medulla (AM) sections

(lower) of *Chat-Cre*, *Cartpt-Cre*, or *Oxtr-Cre* mice injected with AAV8-*hSyn-DIO-mC* (for control) in the SC, observed 2 hours after CNO administration. mC+ axons are shown in magenta. Scale bars, 200 μm for low-magnification images and 50 μm for magnified images. **c**, The fraction of c-Fos+ per DAPI+ cells in the AM of CNO-treated *Gq* and *mC* control male (M) and female (F) mice. Data correspond to Fig. 3**e**; however, data are presented separately for males and females. The number of animals (N) is indicated in blue within the panel. ns, non-significant by a two-sided Welch's *t*-test. Error bars, SD. Source data are provided as a Source Data file.

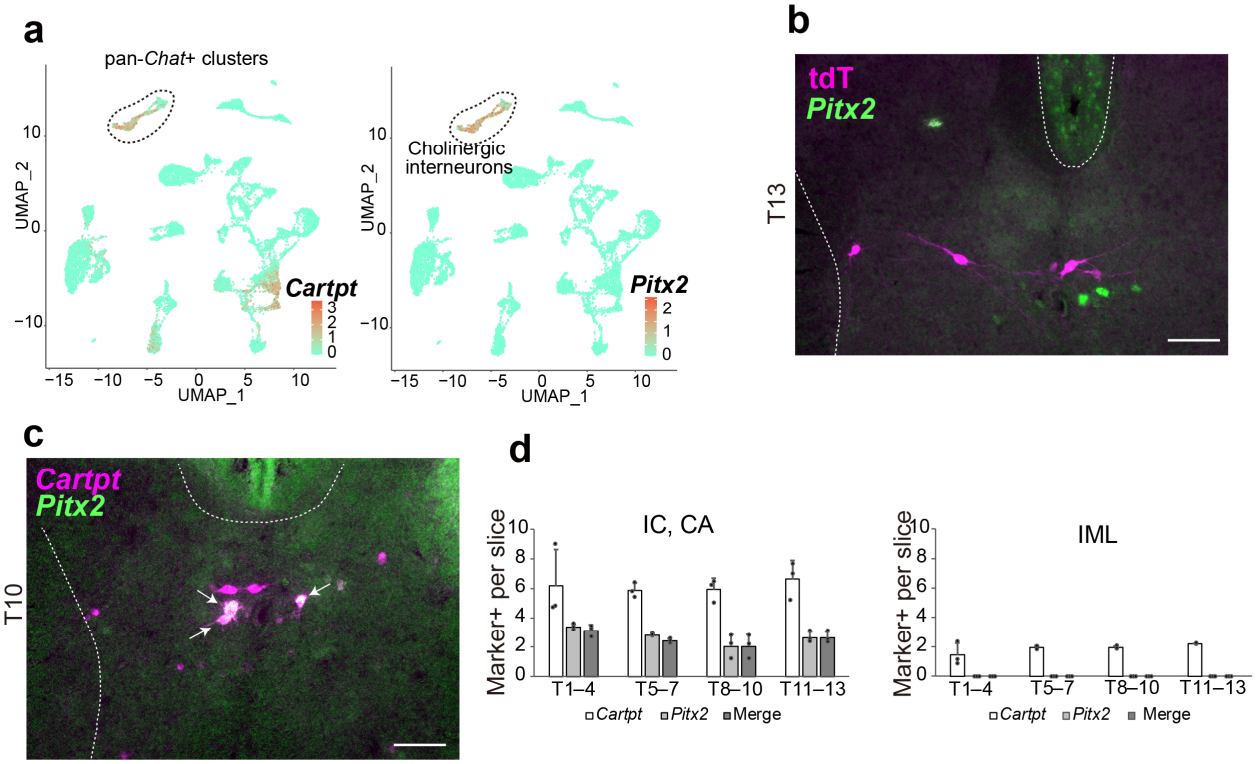

Supplementary Fig. 5: *Cartpt*+ cholinergic interneurons, related to Fig. 4.

a, UMAP representation of pan-*Chat*+ clusters based on the reanalysis of published transcriptome data[2] with a colored heat map showing the log-normalized expression of *Cartpt* (left) and *Paired-like homeodomain 2* (*Pitx2*), a marker of the cholinergic interneurons (right). The dashed line-enclosed clusters represent *Pitx2*+ cholinergic interneurons, which are also *Cartpt*+. **b**, Coronal section of the T13 SC displaying retrogradely labeled tdT+ cells (magenta) from the CG/SMG and *Pitx2* mRNA (green) expression. Scale bars, 100 µm. No overlap was observed. **c**, Expression of *Cartpt* mRNA (magenta) and *Pitx2* mRNA (green) in the T10 SC of wild-type mice. The arrows indicate cells that are double-positive for *Cartpt* and *Pitx2*. Scale bars, 100 µm. **d**, Average number of *Cartpt*+ (white), *Pitx2*+ (light gray), and *Cartpt*+ *Pitx2*+ (dark gray) cells per slice in the IC and CA (left) or IML (right) of the T1–4, T5–7, T8–10, and T11–13 SC segments in wild-type mice. N = 3 mice. Source data are provided as a Source Data file.

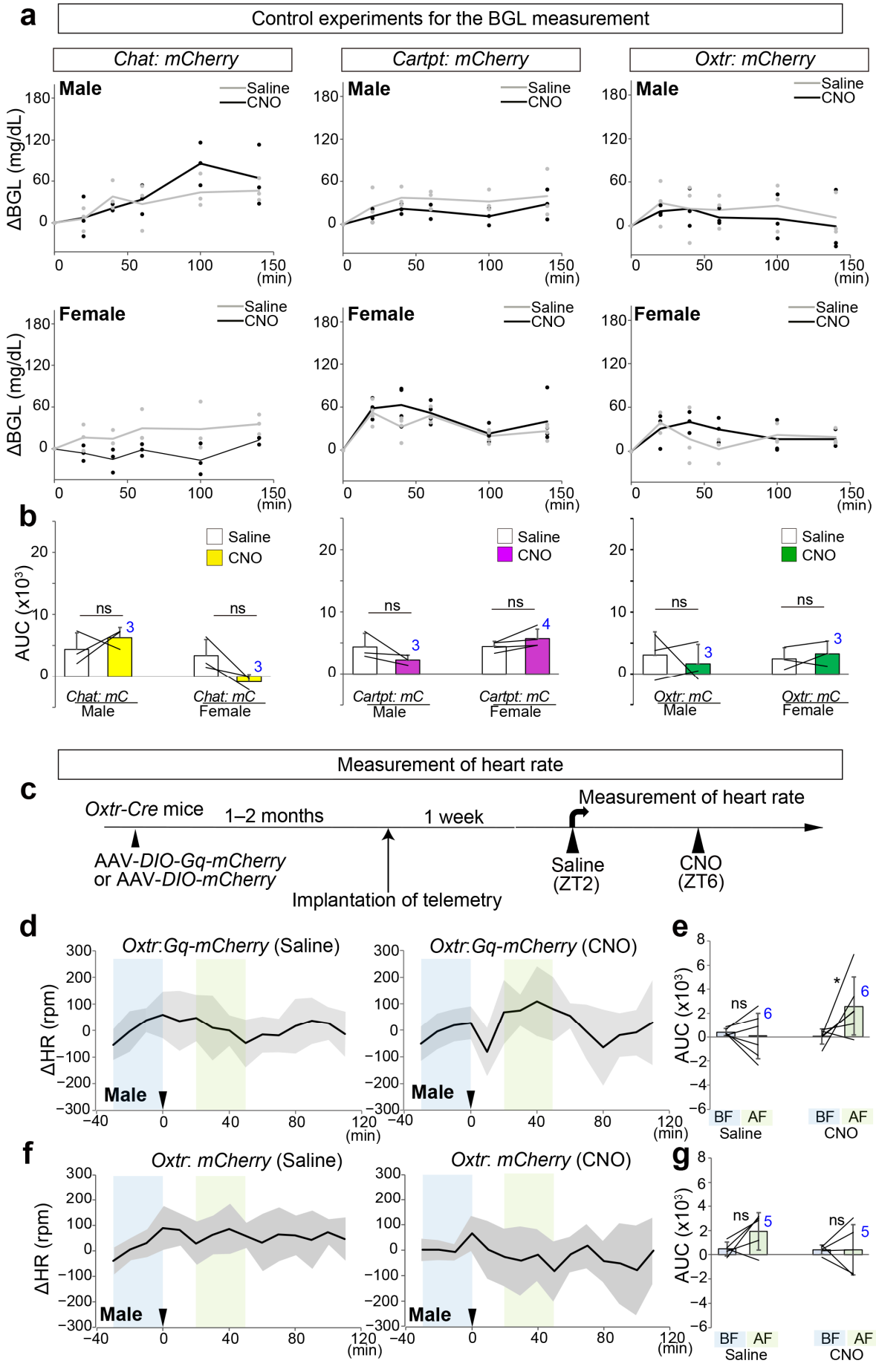
a
Control experiments for the BGL measurement
Chat: mCherry
Cartpt: mCherry
Oxtr: mCherry
Male
Female
Saline
CNO
ΔBGL (mg/dL)
(min)
b
AUC (x10³)
ns
Chat: mC
Cartpt: mC
Oxtr: mC
Male
Female
c
Measurement of heart rate
Oxtr-Cre mice
1–2 months
1 week
AAV-DIO-Gq-mCherry
or AAV-DIO-mCherry
Implantation of telemetry
Saline
(ZT2)
CNO
(ZT6)
d
Oxtr:Gq-mCherry (Saline)
Oxtr:Gq-mCherry (CNO)
ΔHR (rpm)
e
f
Oxtr: mCherry (Saline)
Oxtr: mCherry (CNO)
g
BF
AF

Supplementary Fig. 6: Control data on blood glucose levels and measurement of heart rate, related to Fig. 5.

a, ΔBGL in *Chat-Cre*, *Cartpt-Cre*, or *Oxtr-Cre* mice with AAV8-*hSyn-DIO-mCherry* injection (for control) upon administration of saline (gray) or CNO (black). Individual results are represented by dots, while the average is indicated by a line. The upper and lower graphs depict results for male and female mice, respectively. **b**, AUC measurements for 0 to 140 minutes. Statistical comparisons were made using two-way analysis of variance (ANOVA) with repeated measures; (*Chat-Cre*) sex effect, $p < 0.05$, solution effect, ns, interaction effect, ns. (*Cartpt-Cre*) sex effect, ns, solution effect, ns, interaction effect, ns. (*Oxtr-Cre*) sex effect, ns, solution effect, ns, interaction effect, ns. **c**, Schematics illustrating the measurement of heart rate using a telemetry system. ZT, zeitgeber time, with ZT0 representing 08:00. **d**, **f**, Change in heart rate (ΔHR) in *Oxtr-Cre* male mice injected with AAV8-*hSyn-DIO-Gq-mCherry* (panel **d**) or AAV8-*hSyn-DIO-mCherry* (for control, panel **f**) into the T8–T12 spinal segments, upon administration of saline (left) or CNO (right). The average is indicated by a line, with gray shadows representing the SD. Arrowheads indicate the timing of saline or CNO administration. Light blue and light green areas indicate –30 to 0 minutes and +20 to +50 minutes relative to the saline or CNO administration, respectively. **e**, **g**, AUC measurements for –30 to 0 minutes and +20 to +50 minutes. Two-way ANOVA with repeated measures; (*Oxtr*: *Gq, Oxtr*: *mC*) interaction effect, ns, $*p < 0.05$ by a post hoc two-sided Welch's *t*-test (**e, g**). The number of animals (N) is indicated in blue within the panel. Error bars, SD. Source data are provided as a Source Data file.

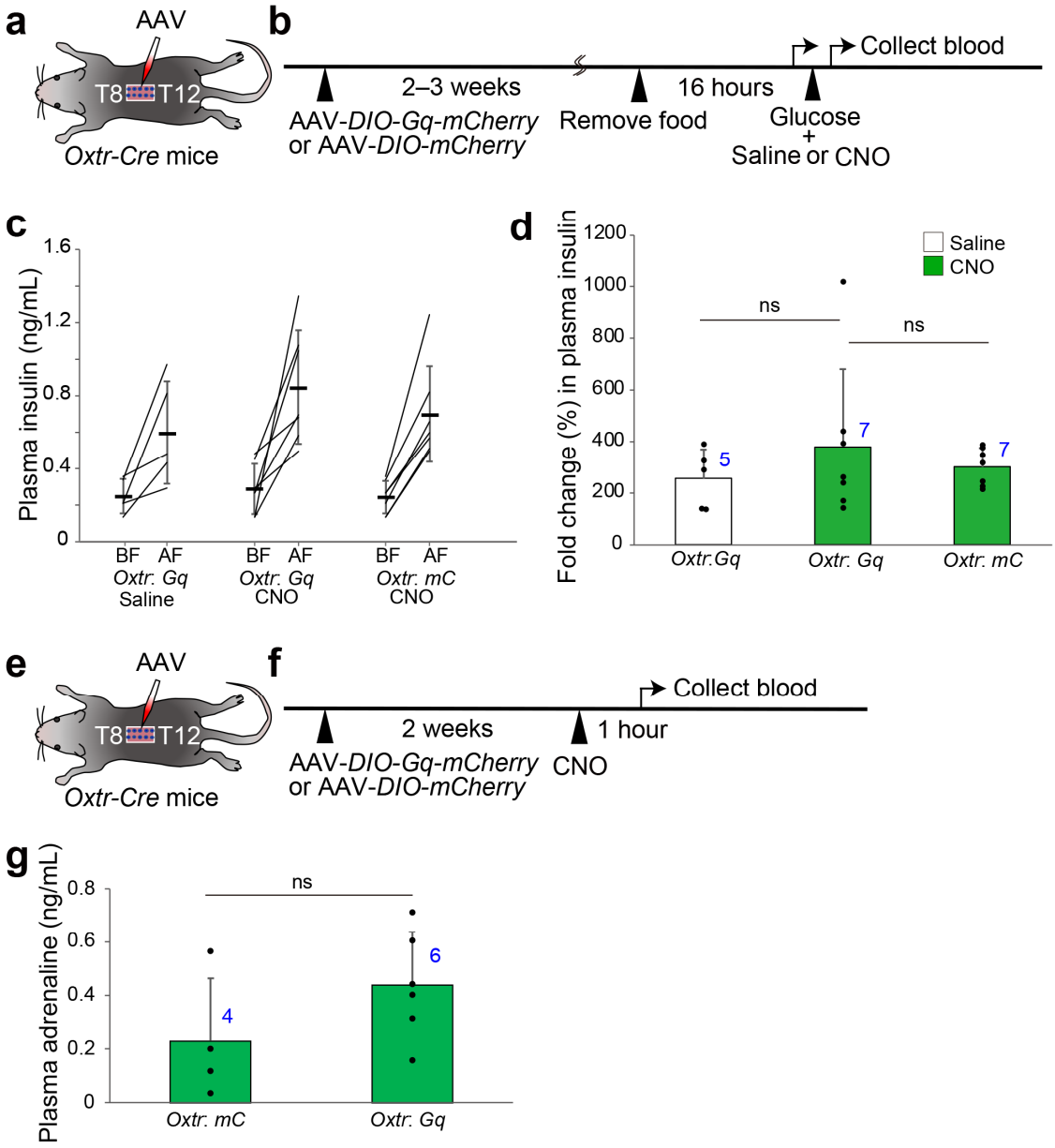

Supplementary Fig. 7: Effect of *Oxtr*+ SPN activation on insulin and adrenaline secretion, related to Fig. 5.

a, **b**, Schematic illustrating the experimental design (**a**) and time line (**b**) for the glucose-stimulated insulin secretion test. **c**, **d**, Plasma insulin levels measured 10 minutes after administration of glucose and either CNO or saline in male *Oxtr*: *Gq* or *Oxtr*: *mC* mice (**c**), along with the corresponding fold change in plasma insulin levels for each condition (**d**). ns, non-significant by one-way analysis of variance. Of note, the 10-minute time point post-CNO administration was chosen based on the literature supporting Gq-mediated activation of PVH Oxt neurons within this time frame[3]. Extending the incubation period following CNO administration may trigger compensatory feedback mechanisms resulting from the elevation of BGLs induced by *Oxtr*+ SPN activation. These data suggest that the observed rise in BGLs following *Oxtr*+ SPN activation is not likely attributable to the suppression of

endogenous insulin secretion. **e**, **f**, Schematic illustrating the experimental design (**e**) and time line (**f**) for plasma adrenaline measurement. **g**, Plasma adrenaline levels measured 1 hour post-CNO administration in male *Oxtr*: *mC* mice and *Oxtr*: *Gq* mice. This time point was selected based on the peak BGLs observed (Fig. 5a). ns, non-significant by a two-sided Welch's *t*-test. The number of animals (N) is indicated in blue within the panel. Error bars, SD. Source data are provided as a Source Data file.

Other Supplementary Materials

Supplementary Table 1: Statistical details and exact p-values.

Supplementary Table 1. Statistical information for Figures			
Figure	Sample size	Analysis	The p-values (before correction)
Fig. 2d (top)	N = 5 for Chat; N = 6 for Cartpt; N = 4 for Oxtr	One-way ANOVA with the post-hoc two-sided Welch's t-test with Bonferroni correction	Chat vs. Cartpt: 8.31 E-1 Chat vs. Oxtr: 2.14 E-2 Cartpt vs. Oxtr: 1.89 E-3
Fig. 2d (middle)	N = 7 for Chat; N = 5 for Cartpt; N = 4 for Oxtr	One-way ANOVA with the post-hoc two-sided Welch's t-test with Bonferroni correction	Chat vs. Cartpt: 9.07 E-4 Chat vs. Oxtr: 1.83 Cartpt vs. Oxtr: 1.68 E-2
Fig. 2d (bottom)	N = 5 for Chat; N = 5 for Cartpt; N = 4 for Oxtr	One-way ANOVA with the post-hoc two-sided Welch's t-test with Bonferroni correction	Chat vs. Cartpt: 1.48 E-9 Chat vs. Oxtr: 3.14 E-4 Cartpt vs. Oxtr: 3.24 E-1
Fig. 3d	N = 8 for Chat-Gq; N = 7 for Chat-mC; N = 4 for Cartpt-Gq; N = 7 for Cartpt-mC; N = 7 for Oxtr-Gq; N = 10 for Oxtr-mC	Two-sided Welch's *t*-test	Chat-Gq vs. Chat-mC: 1.90 E-11 Cartpt-Gq vs. Cartpt-mC: 9.76 E-11 Oxtr-Gq vs. Oxtr-mC: 5.98 E-14
Fig. 3e (top)	N = 10 for Chat-Gq; N = 8 for Chat-mC; N = 8 for Cartpt-Gq; N = 7 for Cartpt-mC;	Two-sided Welch's *t*-test	Chat-Gq vs. Chat-mC: 10.00 E-6 Cartpt-Gq vs. Cartpt-mC: 4.66 E-4 Oxtr-Gq vs. Oxtr-mC: 8.38 E-1

	N = 7 for Oxtr-Gq; N = 10 for Oxtr-mC		
Fig. 3e (bottom)	N = 8 for Chat-Gq; N = 8 for Chat-mC; N = 11 for Cartpt-Gq; N = 7 for Cartpt-mC; N = 9 for Oxtr-Gq; N = 11 for Oxtr-mC	Two-sided Welch's *t*-test	Chat-Gq vs. Chat-mC: 4.39 E-4 Cartpt-Gq vs. Cartpt-mC: 7.31 E-1 Oxtr-Gq vs. Oxtr-mC: 7.50 E-5
Fig. 4c (left)	N = 10 for Chat-Gq; N = 7 for Chat-mC	Two-way ANOVA with the post-hoc two-sided Welch's t-test	Chat-Gq; Saline vs. CNO: 9.25 E-6 Chat-mC; Saline vs. CNO: 6.23 E-2
Fig. 4c (center)	N = 11 for Cartpt-Gq; N = 8 for Cartpt-mC	Two-way ANOVA with the post-hoc two-sided Welch's t-test	Cartpt-Gq; Saline vs. CNO: 3.54 E-11 Carpt-mC; Saline vs. CNO: 1.18 E-1
Fig. 4c (right)	N = 9 for Oxtr-Gq; N = 6 for Oxtr-mC	Two-way ANOVA with the post-hoc two-sided Welch's t-test	Oxtr-Gq; Saline vs. CNO: 1.43 E-1 Oxtr-mC; Saline vs. CNO: 3.66 E-1
Fig. 4e	N = 11 for Cartpt-Gq; N = 7 for Cartpt-Gq (+CGX)	Two-sided Welch's *t*-test	Cartpt-Gq vs. Cartpt-Gq (+CGX): 4.14 E-9
Fig. 4f	N = 4 for Cartpt-Gq (no food)	Two-sided Welch's *t*-test	Saline vs. CNO: 1.65 E-3
Fig. 4h	N = 5	Two-sided Welch's *t*-test	Saline vs. CNO: 1.73 E-2
Fig. 5a (left)	N = 5 for Chat-Gq (male)	Two-way ANOVA with the post-hoc two-sided Welch's t-test with Bonferroni correction	20min; Saline vs. CNO: 2.77 E-2 40min; Saline vs. CNO: 3.49 E-2 60min; Saline vs. CNO: 1.63 E-1 100min; Saline vs. CNO: 1.96 E-1 140min; Saline vs. CNO: 8.41 E-1
Fig. 5a (right)	N = 7 for Oxtr-Gq (male)	Two-way ANOVA with the post-hoc two-sided Welch's t-test with Bonferroni correction	20min; Saline vs. CNO: 2.30 E-2 40min; Saline vs. CNO: 8.02 E-3 60min; Saline vs. CNO: 1.75 E-2 100min; Saline vs. CNO: 8.29 E-2 140min; Saline vs. CNO: 1.56 E-1

Fig. 5b	N = 5 for Chat-Gq (male); N = 6 for Chat-Gq (female); N = 5 for Cartpt-Gq (male); N = 7 for Cartpt-Gq (female); N = 7 for Oxtr-Gq (male); N = 7 for Oxtr-Gq (female)	Two-way ANOVA with the post-hoc two-sided Welch's t-test	Chat-Gq (male); Saline vs. CNO: 2.58 E-2 Chat-Gq (female); Saline vs. CNO: 5.39 E-1 Cartpt-Gq (male); Saline vs. CNO: 8.96 E-1 Cartpt-Gq (female); Saline vs. CNO: 7.15 E-2 Oxtr-Gq (male); Saline vs. CNO: 9.33 E-4 Oxtr-Gq (female); Saline vs. CNO: 1.31 E-1
Fig. 5e	N = 5	Two-sided Welch's *t*-test	Saline vs. CNO: 8.84 E-1
Fig. 6e	N = 5	Two-sided Welch's *t*-test	OT: Gq vs. OT:mC: 9.82 E-3
Fig. 6h	N = 6	Two-sided Welch's *t*-test	Otr: Saline vs. Otr: taCasp: 3.79 E-5
Fig. 6j	N = 8 for OT: Gq, Otr: Saline N = 6 for OT: Gq, Otr: taCasp N = 5 for OT: mC, Otr: Saline	Two-way ANOVA with the post-hoc Wilcoxon's signed-rank test	(OT: Gq, Oxtr: Saline) Saline vs. CNO: 3.57 E-2 (OT: Gq, Oxtr: taCasp) Saline vs. CNO: 9.17 E-1 (OT: mC, Oxtr: Saline) Saline vs. CNO: 1.96
Fig. 7c	N = 6 for 2-DG; N = 6 for Saline	Two-sided Welch's *t*-test	T8-10; 2-DG vs. Saline: 6.48 E-5 T11-13; 2-DG vs. Saline: 2.68 E-4
Fig. 7f	N = 6 for Oxtr+; N = 6 for Cartpt+	Two-sided Welch's *t*-test	T8-10; Oxtr vs. Cartpt: 4.77 E-3 T11-13; Oxtr vs. Cartpt: 4.32 E-3
Ex Fig. 4c	N = 4 for Chat-Gq (male) N = 4 for Chat-Gq (female) N = 5 for Oxtr-Gq (male) N = 4 for Oxtr-Gq (female)	Two-sided Welch's *t*-test	Chat-Gq: male vs. female: 6.13 E-1 Oxtr-Gq: male vs. female: 9.66 E-2
Ex Fig. 6b	N = 3 for Chat-mC (male); N = 3 for Chat-mC (female); N = 3 for Cartpt-mC (male); N = 4 for Cartpt-mC (female); N = 3 for Oxtr-mC (male); N = 3 for Oxtr-mC (female)	Two-way ANOVA with the post-hoc two-sided Welch's t-test	Chat-mC (male); Saline vs. CNO: 3.73 E-1 Chat-mC (female); Saline vs. CNO: 8.73 E-2 Cartpt-mC (male); Saline vs. CNO: 2.07 E-1 Cartpt-mC (female); Saline vs. CNO: 2.11 E-1 Oxtr-mC (male); Saline vs. CNO: 6.39 E-1 Oxtr-mC (female); Saline vs. CNO: 6.23 E-1

Ex Fig. 6e	N = 6 for Oxtr-Gq (male)	Two-way ANOVA with the post-hoc two-sided Welch's t-test	Saline; Before vs. After: 7.18 E-1 CNO; Before vs. After: 4.74 E-2
Ex Fig. 6g	N = 5 for Oxtr-mC (male)	Two-way ANOVA with the post-hoc two-sided Welch's t-test	Saline; Before vs. After: 1.05 E-1 CNO; Before vs. After: 9.96 E-1
Ex. Fig. 7d	N = 5 for Oxtr: Gq (Saline) N = 7 for Oxtr: Gq (CNO) N = 7 for Oxtr: mC (CNO)	One-way ANOVA with the post-hoc two-sided Welch's t-test with Bonferroni correction	Oxtr: Gq (Saline) vs. Oxtr: Gq (CNO): 1.09 Oxtr: Gq (CNO) vs. Oxtr: mC (CNO): 2.59
Ex. Fig. 7g	N = 4 for Oxtr-mC (male) N = 6 for Oxtr-Gq (male)	Two-sided Welch's *t*-test	Oxtr: mC vs. Oxtr: Gq: 1.93 E-1

Supplementary References

1. Abe T, Inoue KI, Furuta Y, Kiyonari H. Pronuclear Microinjection during S-Phase Increases the Efficiency of CRISPR-Cas9-Assisted Knockin of Large DNA Donors in Mouse Zygotes. *Cell Rep* **31**, 107653 (2020).

2. Blum JA*, et al.* Single-cell transcriptomic analysis of the adult mouse spinal cord reveals molecular diversity of autonomic and skeletal motor neurons. *Nat Neurosci* **24**, 572-583 (2021).

3. Papazoglou I*, et al.* A distinct hypothalamus-to-beta cell circuit modulates insulin secretion. *Cell Metab* **34**, 285-298 e287 (2022).